Cholesterol Monohydrate Nucleation in Ultrathin Films on Water

Hanna Rapaport,* Ivan Kuzmenko,* Sylvaine Lafont,* Kristian Kjaer,† Paul B. Howes,† Jens Als-Nielsen,‡ Meir Lahav,* and Leslie Leiserowitz*

*Department of Materials and Interfaces, Weizmann Institute of Science, Rehovot 76100, Israel; †Materials Research Department, Risø National Laboratory, DK-4000 Roskilde, Denmark; and ‡Niels Bohr Institute, H. C. Ørsted Laboratory, DK-2100 Copenhagen, Denmark

ABSTRACT The growth of a cholesterol crystalline phase, three molecular layers thick at the air-water interface, was monitored by grazing incidence x-ray diffraction and x-ray reflectivity. Upon compression, a cholesterol film transforms from a monolayer of trigonal symmetry and low crystallinity to a trilayer, composed of a highly crystalline bilayer in a rectangular lattice and a disordered top cholesterol layer. This system undergoes a phase transition into a crystalline trilayer incorporating ordered water between the hydroxyl groups of the top and middle sterol layers in an arrangement akin to the triclinic 3-D crystal structure of cholesterol · H_2O. By comparison, the cholesterol derivative stigmasterol transforms, upon compression, directly into a crystalline trilayer in the rectangular lattice. These results may contribute to an understanding of the onset of cholesterol crystallization in pathological lipid deposits.

INTRODUCTION

Cholesterol (Scheme 1), the most abundant sterol in animal tissues, is a component of cell membranes, plasma lipoproteins, and a precursor in the biosynthesis of bile salts and hormones. Recently, evidence has accumulated that, other than controlling the mechanical properties of cell membranes, cholesterol, together with sphingolipids form organized domains, lipid rafts (Brown and London, 1998; Simons and Ikonen, 2000) that participate in distributing proteins to the cell surface, cell signal transduction, and activation of immune responses. Abnormally high physiological levels of cholesterol may develop into detrimental precipitants containing cholesterol crystallites that are associated with atherosclerotic plaques (Small and Shipley, 1974; Small, 1998; Guo et al., 2000) and with gallstones in the bile (Bogren and Larsson, 1963). Various studies on cholesterol crystallization in model or native bile solutions by light and electron microscopy and synchrotron x-ray diffraction (Konikoff et al., 2000, 1997; Kaplun et al., 1994; Wang and Carey, 1996; Somjen et al., 1995) have provided evidence that crystallites form through aggregation of cholesterol-rich vesicles. Furthermore, an x-ray powder diffraction pattern obtained from early-formed filamentous crystallites of cholesterol in bile solution has been interpreted as possibly depicting an unknown crystalline polymorph of cholesterol (Konikoff et al., 1992). Recently, by employing the method of grazing incidence x-ray diffraction (Als-Nielsen and Kjaer, 1989; Jacquemain et al., 1992; Rapaport et al., 2000), we have shown that cholesterol crystallizes on a water surface in monolayer and bilayer phases (Lafont et al., 1998) that are different from the known three-dimensional (3-D) structures (Craven, 1976; Shieh et al., 1977; Hsu and Nordman, 1983).

Here we provide evidence for cholesterol monohydrate crystallites, three molecular layers thick, evolving from a film containing the cholesterol monolayer and bilayer 2-D crystalline phases. Structural models of the three phases as well as a mechanism of the phase transition are presented. The formation and structure of crystalline thin films of cholesterol analogs, stigmasterol and cholesteryl acetate (Scheme 1), are described here, but in brief. The surface x-ray scattering studies of cholesterol acetate and stigmasterol and the structure determination of the macroscopic 3-D crystal form of stigmasterol hemihydrate shall be published separately in a future paper.

MATERIALS AND METHODS

Cholesterol, stigmasterol, and cholesterylacetate of the highest purity available were obtained from Sigma (St. Louis, MO). Lipid/chloroform solutions (~0.1 mg/ml) were used to form the monolayer films at the air-water interface for surface-pressure versus area (π-A) isotherms and x-ray diffraction measurements.

A detailed description of grazing incidence x-ray diffraction (GIXD) applied to films on liquid surfaces has been given elsewhere (Als-Nielsen and Kjaer, 1989; Jacquemain et al., 1992; Rapaport et al., 2000). The GIXD experiments described here were performed on the liquid surface diffractometer at the undulator BW1 beam line at the HASYLAB synchrotron source, Desy (Hamburg, Germany). The films were spread at room temperature, and diffraction measurements were performed at 5°C. A monochromatic x-ray beam (λ = 1.3037 Å) was adjusted to strike the liquid surface at an incident angle ($\alpha < 0.85\alpha_c$ where α_c is the critical angle for total external reflection), which maximizes surface sensitivity. The dimensions of the footprint of the incoming x-ray beam on the liquid surface were ~5 × 50 mm. GIXD signals were obtained from 2-D crystallites randomly oriented about the water surface normal in the form of a 2-D powder. The scattered intensity was collected by means of a position-sensitive detector (PSD) which intercepts photons over the range $0.0 < q_z < 0.9$ Å^{-1}, q_z being the out-of-plane component of the scattering vector. Measurements were performed by scanning the horizontal component, $q_{xy} \approx 4\pi\sin\theta_{xy}/\lambda$, of the scattering vector, where $2\theta_{xy}$ is the angle between the incident and diffracted beam projected onto the horizontal plane. The diffraction data are represented in two ways: 1) The GIXD

Received for publication 26 March 2001 and in final form 14 June 2001.

Address reprint requests to Dr. Leslie Leiserowitz, Department of Materials and Interfaces, The Weizmann Institute of Science, Rehovot 76100, Israel. Tel.: 972-8-934-3727; Fax: 972-8-934-4138; E-mail: leslie.leiserowitz@weizmann.ac.il.

0006-3495/01/11/2729/08 $2.00

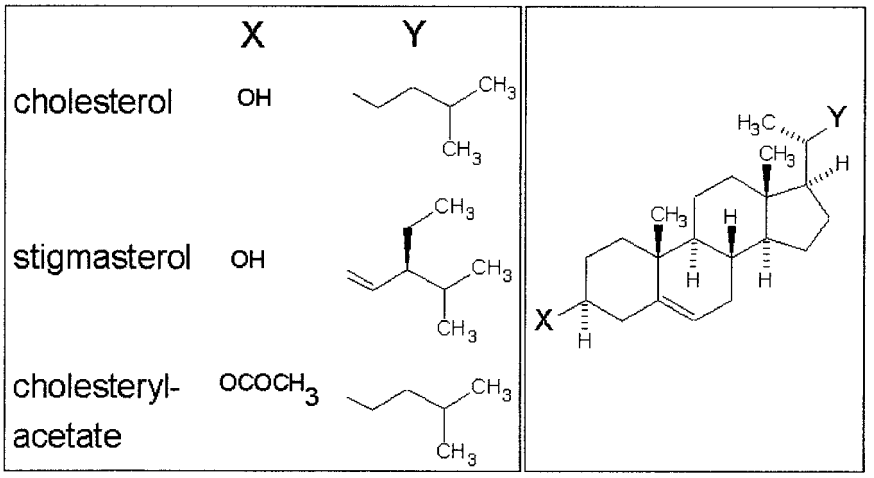

Scheme 1

pattern $I(q_{xy})$, obtained by integrating over the whole q_z window of the PSD, shows Bragg peaks; 2) Bragg rod intensity profiles are the scattered intensity $I(q_z)$ recorded in channels along the PSD but integrated across the q_{xy} range of each Bragg peak. The q_{xy} positions of the Bragg peaks yield the lattice repeat distances $d = 2\pi/q_{xy}$, which may be indexed by the two Miller indices h,k to yield the unit cell. The full width at half-maximum (FWHM) of the Bragg peaks yields the lateral 2-D crystalline coherence length $L_{xy} \approx 0.9(2\pi)/\mathrm{FWHM}(q_{xy})$.

For vertically homogeneous monolayers (or for thick and thus, again, vertically homogeneous) multilayers (say, more than 10 layers), the width of the Bragg rod profile along q_z similarly gives a measure of the thickness of the crystalline film $L_z \approx 0.9(2\pi)/\mathrm{FWHM}(q_z)$. For the few-layer films encountered in this work, L_z thus calculated may be used in some cases as a first guide. Generally, the intensity at a particular value of q_z in a Bragg rod is proportional to the square of the molecular structure factor, $|F_{hk}(q_z)|^2$. Thus Bragg rod intensities for the proposed models can be calculated using the atomic coordinates in the unit cell.

To apply the SHELX-97 computer program (Sheldrick, 1997) designed for 3-D crystals to refine a 2-D crystal structure of a powder, oriented with respect to the water surface but randomly oriented around the normal to the surface, the following procedure was adopted. The Bragg rod intensities $F^2(h, k, q_z)$ were assigned l Miller indices according to a virtual c axis ($\sim$500 Å) to transform a continuous $F^2(h, k, q_z)$ distribution along q_z, into a discrete $F^2(h, k, l)$ reflection data set corresponding to the virtual 3-D crystal. The superposition of the $F^2(h, k, q_z)$ and $F^2(-h, -k, q_z)$ Bragg rods, a property of the measured GIXD pattern because the sample on water consists of a 2-D crystalline powder, was simulated in SHELX-97 by imposing a twinning of the crystal about the ab plane. Given the limited amount of observed diffraction data, refinement of the sterol structures is possible only by applying restraints and constraints to the molecular structure and intermolecular contacts. The CERIUS^2 computational package (Molecular Simulations, San Diego. CA) was used for the construction of the molecular models.

Whereas GIXD, described above, picks up a signal from any laterally ordered parts of the thin film, specular x-ray reflectivity (XR) results from the electron density contrast between the air above and the subphase below. For an ideally sharp interface between the two media, the result would be $R(q_z) = R_F(q_z)$, the Fresnel law of optics. When the vertical electron density variation, $\rho(z)$, is modulated by a thin film at the interface, the reflectivity ratio $R(q_z)/R_F(q_z)$ deviates from unity and can be inverted by least-squares fitting a parameterized model $\rho(z)$. A convenient model comprises multiple slabs of thicknesses L_i and (constant) densities ρ_i calculated from molecular vertical distances, corresponding numbers, Z_i, of electrons and the area per molecule, A. Finally, the $\rho(z)$ model is smeared by convolution with a Gaussian, $\exp(-z^2/(2\sigma^2))$. The reflectivity ratio $R(q_z)/R_F(q_z)$ will be expressed as a function of q_z/q_c, $= \sin\alpha/\sin\alpha_c$, where α_c is the critical angle for total external reflection (vide supra).

RESULTS AND DISCUSSION

Cholesterol films were formed on water and their GIXD patterns measured at several points along the surface pressure-molecular area (π-A) isotherm (Fig. 1 *A*, *inset*). At a nominal area per molecule of $A = 50$ Å^2, a broad Bragg peak (Fig. 1 *A*, curve *a*) with a d spacing of 5.7 Å was detected and assigned to a hexagonal unit cell $a = b = 6.6$ Å, area $ab\sin\gamma = 37.7$ Å^2. This relatively broad Bragg peak, which could not always be traced within the region of the film scanned (5×50 mm^2) by the x-ray beam (see Materials and Methods), indicates crystalline aggregates, of average diameter $L_{xy} = 100$ Å, i.e., comprising $\sim$200 molecules, in coexistence with an amorphous monolayer phase. The Bragg rod associated with this Bragg peak has a shape and FWHM (see Materials and Methods) corresponding to a monolayer of molecules oriented normal to the plane of the water surface. In the liquid-crystalline state of hydrated cholesterol (Loomis et al. 1979), which exists over the temperature range between 124°C and 157°C, a diffuse diffraction peak with a spacing of $\sim$5.7 Å was observed. On the assumption that the monolayer peak of cholesterol arises from a free-rotator phase as in amphiphilic acids and alcohols (Shih et al., 1992), the molecule would lie in a hexagonal unit cell $a = b = 6.6$ Å, area $ab\sin\gamma = 37.7$ Å^2. According to molecular modeling (see Materials and Methods), such a free-rotator phase would have led to short repulsive intermolecular contacts. An alternative model was constructed, which consists of a supercell $a' = b' = \sqrt{3}a = 11.4$ Å with acceptable intermolecular distances, containing three molecules related by threefold symmetry in the plane group $p3$ (Fig. 1 *C*). This molecular arrangement yields a good agreement between the observed and calculated GIXD

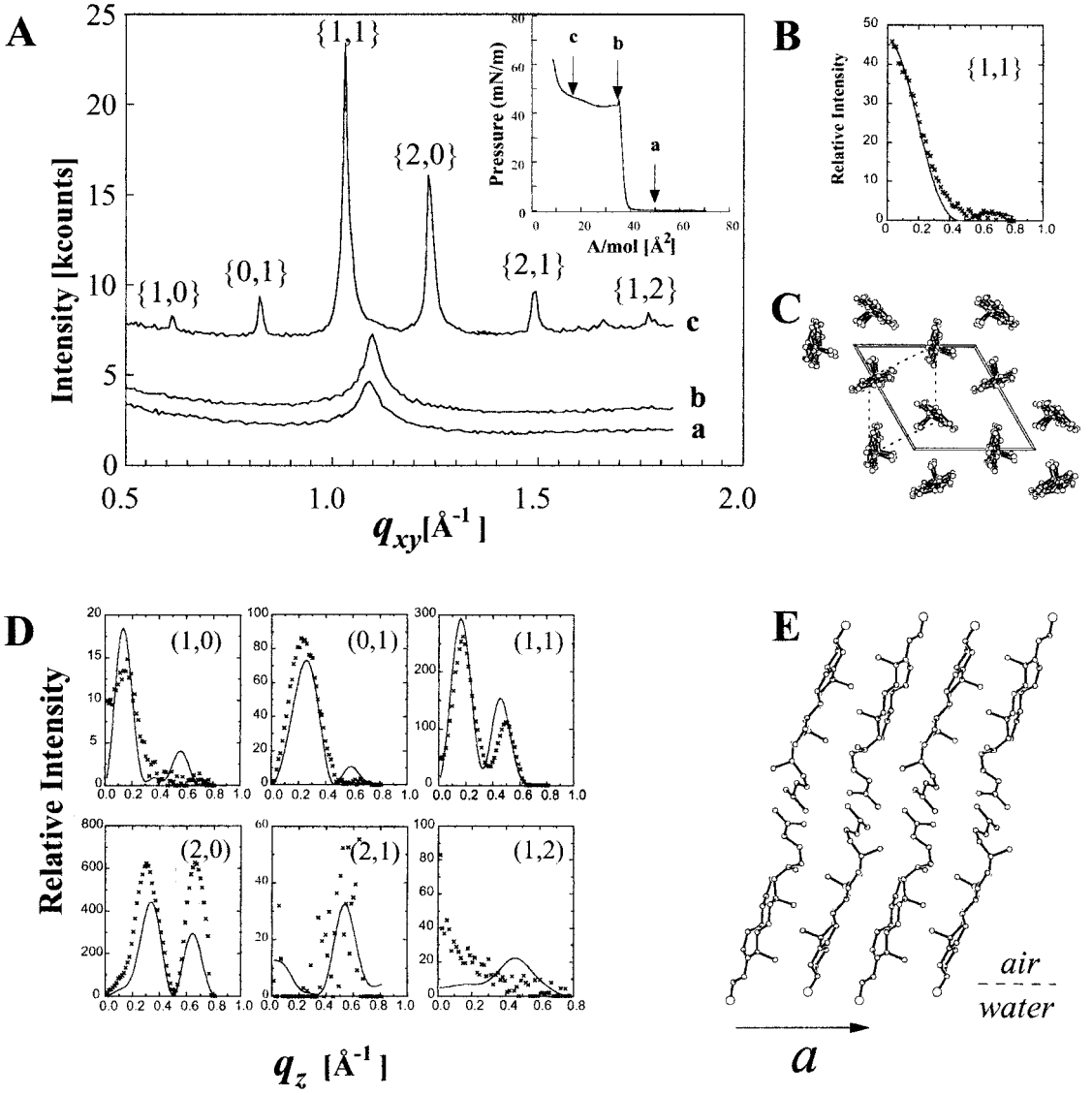

FIGURE 1 (*A*) GIXD patterns $I(q_{xy})$ of cholesterol film on the water surface at points *a*-*c* along the π-*A* isotherm shown in inset. (*B*) The observed ($\times$) and calculated (——) Bragg rod $I(q_z)$ at $I(q_{xy}) = 1.1$ Å^{-1} in scan *b*. (*C*) The proposed cholesterol monolayer structure, of trigonal symmetry *p*3, that yields the calculated {1,1} Bragg rod (——) shown in *B*. The molecules are arranged in an $a'b'$ super cell (——) constructed from the subcell ($\cdots$). The validity of the model is also supported by the absence, in the calculated diffraction pattern of the q_{xy} region scanned by GIXD, of additional Bragg peaks with an intensity >5% of the {1,1} Bragg peak, in agreement with the non-observation of additional peaks. (*D*) The observed ($\times$) and calculated (——) Bragg rod profiles $I(q_z)$ corresponding to the Bragg peaks in scan *c*. The {*h*, *k*} assignment of the Bragg peaks corresponds to a rectangular 10.1 $\times$ 7.6 Å^2 *ab* unit cell. (*E*) The model bilayer structure of the 10.1 $\times$ 7.6 Å^2 cell, viewed along the *b* axis that yields the calculated Bragg rod profiles (lines in *D*). The two layers are related by 2_1-symmetry parallel to the *b* axis. The bilayer model, which contains two crystallographically independent cholesterol molecules, was refined by x-ray structure-factor least-squares with constraints and restraints imposed on the rigid and flexible moieties of the cholesterol molecule.

intensity patterns. The best fit to the observed Bragg rod (Fig. 1 *B*) was achieved assuming the exocyclic octyl moiety is highly disordered (i.e., instead of applying high-temperature factors to the disordered atoms of the exocyclic octyl moiety, which excludes the C atom bound to the rigid sterol skeleton, these atoms were not included in the x-ray structure-factor calculations). In this assembly, the molecules are able to librate about their long axes in a cooperative manner resulting in a hindered-rotator phase. In this way, it is possible to reconcile the diffraction results of the liquid-crystalline phase of cholesterol at high temperatures with the cholesterol monolayer phase at 5°C.

The Bragg peaks corresponding to the cholesterol bilayer in the rectangular cell $a = 10.07$ Å, $b = 7.57$ Å, area $ab = 76.2$ Å^2, indicating two sterol molecules in the cell within a layer, were observed after compressing the monolayer film beyond the collapse point to $A = 16$ Å^2 (Fig. 1 *A*). The widths of these peaks, decidedly narrower than those of the

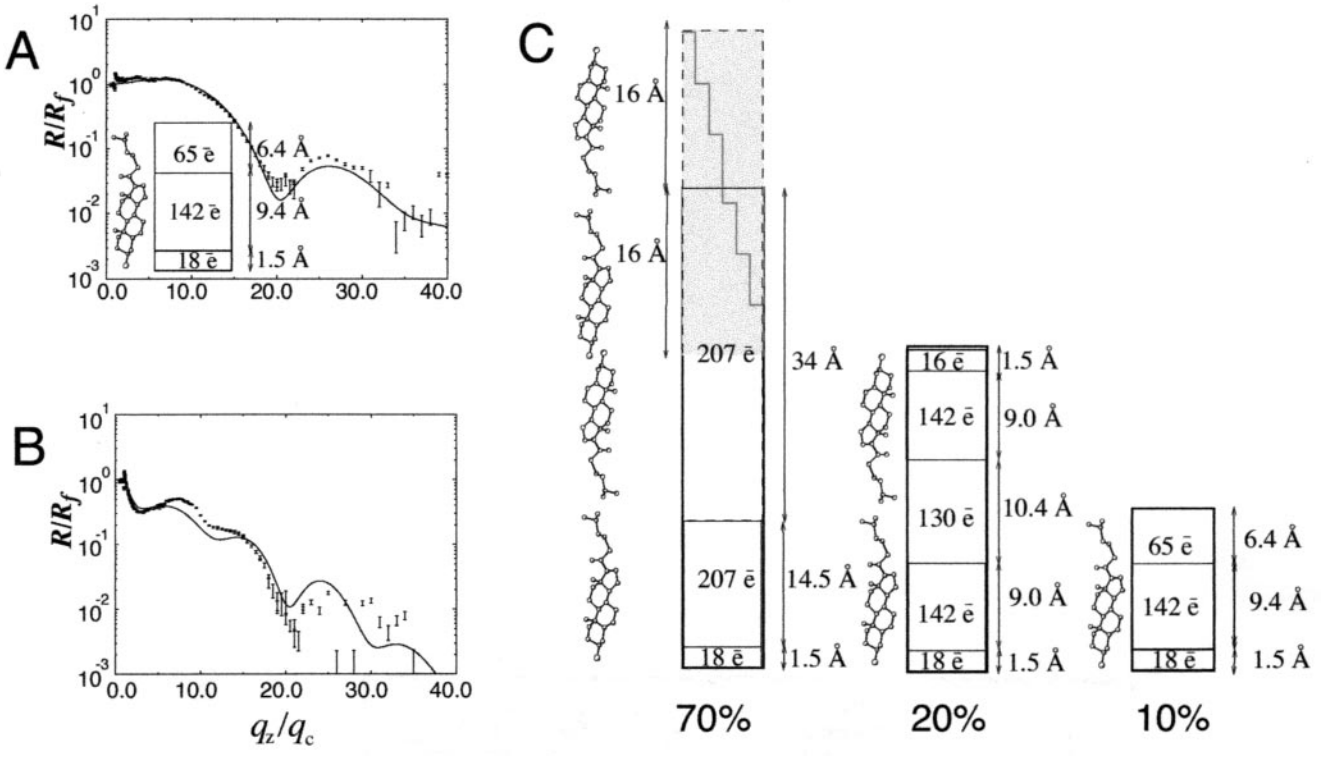

FIGURE 2 Observed (×) and calculated (——) x-ray reflectivity (XR) curves of cholesterol (*A* and *B*) films on water at areas per molecule $A = 40$ Å^2 (*A*) and 16 Å^2 (*B*). These curves are presented in the form of R/R_f as a function of q_z/q_c, (See Materials and Methods). The measured XR curve at $A = 40$ Å^2, were modeled by least-squares assuming a steroid monolayer in the form of the depicted slab model divided into three parts, each with fixed height L_I (from the GIXD analysis) and electron density $L_i Ne_i/A$, where Ne_i is the number of electrons in slab *i* and *A* the area covered by the molecule according to the unit cell area from the GIXD analysis (e). The parameters adjusted were surface roughness (σ), yielding a reasonable value of 2.5 Å and the number of electrons in the box closest to the water surface assuming a box height of 1.5 Å being composed of the steroid OH group comprising 9e, and partial water occupancy. The observed XR curves at $A = 16$ Å^2 were best fitted assuming coexistence of three phases. The three corresponding models are depicted: a trilayer with a rough upper surface comprised of three slabs, a smooth bilayer composed of five slabs, and a monolayer, each model with fixed heights L_i and electron densities $L_i Ne_i/A$ taken from the GIXD analysis. The only parameters adjusted were σ for the rough upper surface of the trilayer of cholesterol, yielding a value σ = 16 Å that corresponds to the length of a cholesterol molecule, and the relative percentage occupancies of the three model structures 7:2:1 as shown. The surface roughness σ of 16 Å for the trilayer is depicted by stepped lines indicating a variation in film thickness ranging approximately from two to four layers.

monolayer phase, yield crystalline bilayer domains of average size $L_{xy} = 370$ Å, thus comprising ~5600 molecules. The rectangular nature of the cell implies twofold (2) or twofold screw (2_1) symmetry relating the two layers; in fact, the latter symmetry element, directed along the *b* axis, is evident from the very low intensity of the (0, 1) Bragg rod at $q_z = 0$ Å^{-1} (Fig. 1 *D*). A molecular model of the bilayer (Fig. 1 *E*), refined using the x-ray structure-factor least-squares program SHELX-97 (Sheldrick, 1997) but applied to 2-D crystals on water (see Materials and Methods), gave a reasonable fit between the observed and calculated Bragg rod profiles (see Fig. 1 *D*). The tendency of cholesterol to form a bilayer far more crystalline than the monolayer highlights the role of the interlayer contacts between the exocyclic octyl moieties toward enhancing molecular order. This molecular intralayer arrangement is similar to that found in the 3-D crystals of several long-chain esters of cholesterol (Craven, 1986) but distinctly different from the monohydrate (Craven, 1976) or the anhydrous bulk phases of cholesterol (Shieh et al., 1977; Hsu and Nordman, 1983). We note that the two strongest reflections from the bilayer (Fig. 1 *A*, curve *c*), the {2,0} and {1,1}, have almost the same lattice *d*-spacings (5.0 and 6.0 Å) as the two observed Bragg reflections from the x-ray powder-pattern of early-formed filamentous crystals of cholesterol (4.9 and 5.9 Å) found in bile (Konikoff et al., 1992).

The cholesterol film thickness has been monitored also by x-ray reflectivity (XR) measurements. According to an analysis of the XR data at a surface area $A = 40$ Å^2, the cholesterol molecules form a monolayer (Fig. 2 *A*), in which they are aligned upright on the water surface, in agreement with the analysis of the GIXD data. The XR curve of the compressed cholesterol film at $A = 16$ Å^2 (Fig. 2 *B*) could be fitted with an electron slab model of a film composed of a cholesterol trilayer with a rough upper surface, a smooth bilayer, and a monolayer, with a relative surface coverage of

7:2:1 (Fig. 2 *C*). The XR and GIXD results for cholesterol together indicate that the diffraction from the crystalline bilayer arises from both the trilayer with the rough upper surface and the smooth bilayer. The crystalline bilayer is mostly, ~80%, covered by a layer of cholesterol molecules aligned upright, but not ordered in the *ab* plane; the remaining 20% is not covered by the amorphous cholesterol layer.

Stigmasterol (Scheme 1) on water has structural properties somewhat similar to that of cholesterol, as established via GIXD data. At 40 Å^2 the monolayer also forms ordered clusters of low crystallinity and packs via trigonal plane symmetry. In the compressed state, the stigmasterol forms 2-D crystallites three layers thick, arranged in a 10.2 × 7.7 Å^2 layered structure similar to cholesterol (Fig. 1 *E*), but incorporating an ordered hydration layer with three water molecules per sterol adjoining the hydroxyl groups of two neighboring layers related by 2_1-symmetry (Fig. 3 *A*), according to a constrained x-ray structure least-squares refinement of the Bragg rod data as described in the legend to Fig. 3 *A*. The packing of stigmasterol in the trilayer is similar to that of its macroscopic 3-D crystalline form (Fig. 3 *B*) but is a hemihydrate, as determined from a single crystal x-ray structure study (a complete description shall be published separately in a future paper).

The steroid headgroup type may have dramatic effect on the crystallization. Cholesterylacetate (Scheme 1 *C*), as found by GIXD, forms, already in the uncompressed state, a monolayer incorporating a pseudo-rectangular lattice, a = 10.14 Å, b = 7.58 Å, γ = 92.2°, that is more crystalline than the trigonal monolayer phase of cholesterol, as made manifest by relatively high Bragg peak intensities and large crystalline coherence lengths.

The observation that the molecular arrangement of the stigmasterol crystalline trilayer is similar to that of its 3-D macroscopic counterpart led us to examine whether the compressed trilayer film of cholesterol, composed of a crystalline bilayer covered by a disordered layer, would evolve into a trilayer crystal. In a series of three decompression-compression cycles performed on the film (between A = 16 Å^2 and 50 Å^2) the crystallites of the rectangular phase were always found to decompose upon film expansion and reform in the compressed state, implying reversible weak interactions between the crystalline layers. Yet, the compressed film that underwent the hysteresis cycles revealed the formation of three additional Bragg peaks marked in Fig. 4 *A*, bottom scan. After two more hours, during which the film area was kept unchanged, these peaks doubled in intensity (Fig. 4 *A*, top scan) whereas the {1,0} and {0,1} Bragg peaks of the rectangular bilayer phase (not shown) became weaker by ~70%.

The q_{xy} and the q_z positions of the intensity modulations of the newly formed Bragg rods (Fig. 4, *A* and *B*) could be assigned (h, k, l) indices according to the 3-D crystal lattice of the cholesterol monohydrate structure (a = 12.39, b = 12.41, c = 34.4 Å, α = 91.9, β = 98.1, γ = 100.8°)

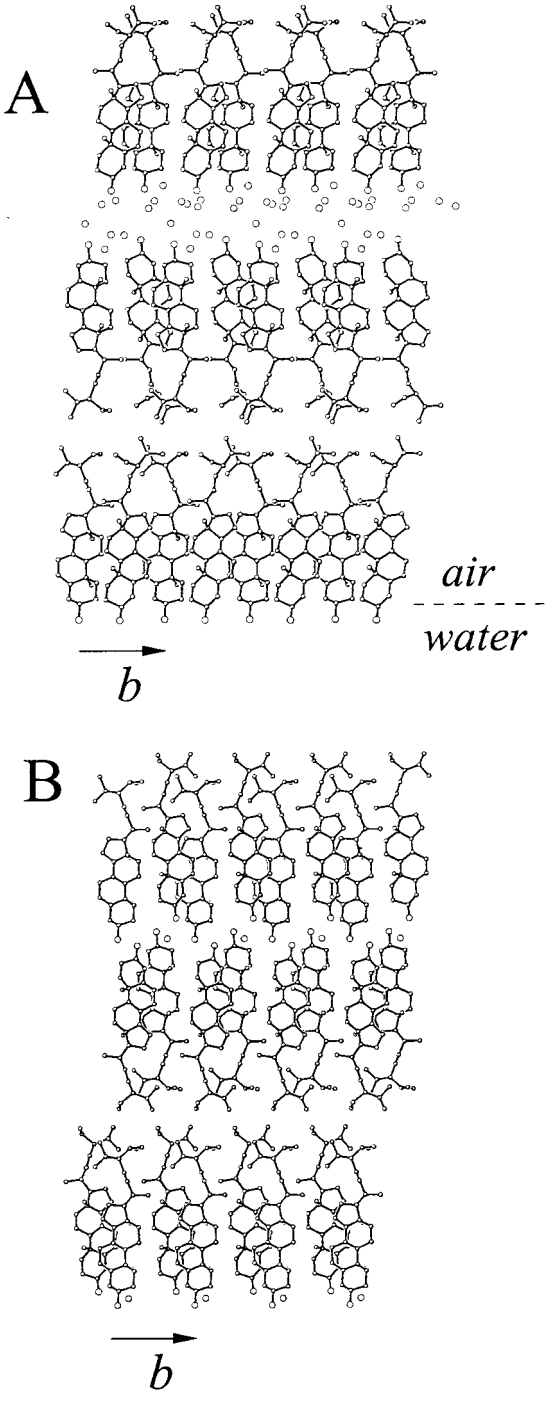

FIGURE 3 (*A*) Model of the trilayer packing arrangement of stigmasterol on a water surface as refined by constrained-restrained x-ray structure-factor least-squares, making use of the GIXD measurements. The structure viewed along a incorporates an ordered layer of water molecules, the space between the top surface of the bilayer and the lower surface of the overlying cholesterol layer being sufficient for the insertion of three waters per sterol with reasonable intermolecular distances. (*B*) View of a trilayer in the 3-D crystal structure of stigmasterol hemihydrate, which packs in the unit cell of dimensions a = 9.5, b = 7.6, c = 36.9 Å, $\alpha = \gamma = 90°$, β = 94.3°, space group $p2_1$. The water molecules in *A* and *B* are depicted by unconnected circles.

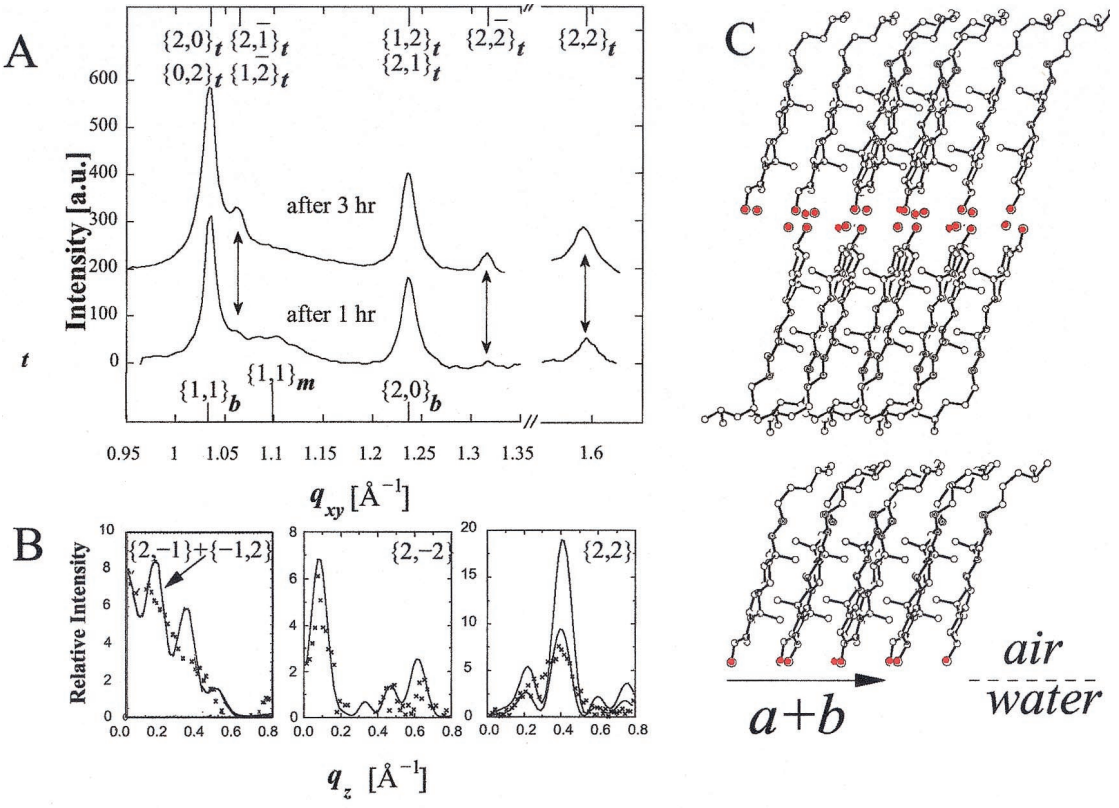
A
{2,0}t {2,1̄}t
{0,2}t {1,2̄}t
{1,2}t
{2,1}t
{2,2̄}t
{2,2}t
Intensity [a.u.]
after 3 hr
after 1 hr
t
{1,1}b
{1,1}m
{2,0}b
0.95 1 1.05 1.1 1.15 1.2 1.25 1.3 1.35 1.6
qxy [Å−1]
B
Relative Intensity
{2,−1}+{−1,2}
{2,−2}
{2,2}
qz [Å−1]
C
air
water
a+b

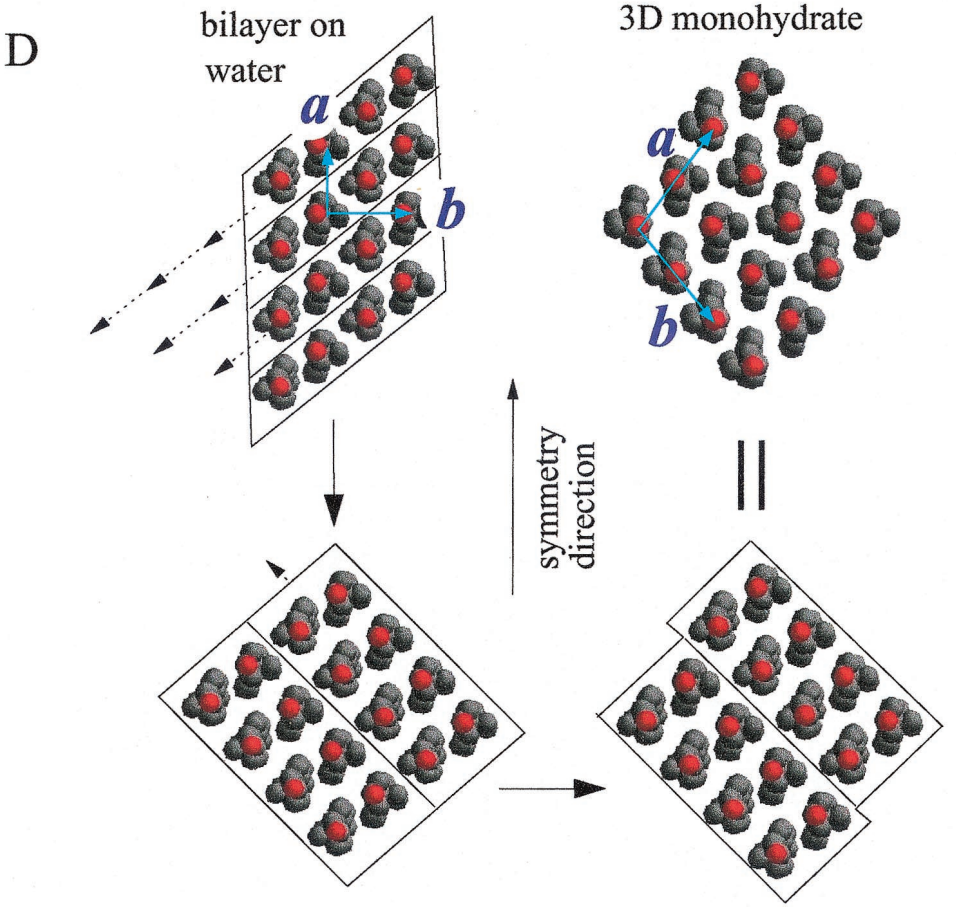
D
bilayer on water
3D monohydrate
a
b
a
b
symmetry direction

(Craven, 1976). The FWHM of the two newly formed Bragg rods $\{2, 2\}_t$ and $\{2, -2\}_t$ indicate a crystalline film ~50 Å thick, corresponding to about three layers. Indeed, Bragg rods calculated using atomic coordinates of a trilayer segment of the monohydrate crystal structure (Fig. 4 *C*) fit the observed data well (Fig. 4 *B*). The Bragg rod of the $\{2, -1\}_t + \{1, -2\}_t$ superimposed reflections of the newly formed phase (Fig. 4, *A* and *B*), but which has the shape corresponding to that of a single layer, can be understood in terms of the pseudo-symmetry of the trilayer structure. Neighboring cholesterol layers in the 3-D crystal structure of the monohydrate are related by pseudo-twofold symmetry about the direction *a*-*b*. Each layer contains four molecules within the cell, two of which are related to the other two by pseudo-translation of 0.5*a* or 0.5*b*. Thus, in a trilayer, the top and bottom layers contain molecules related by the same pseudo-translation axis, say 0.5*a*, whereas in the central layer they are related by 0.5*b*, or the reverse. Consequently we envisage two trilayer structures on the water, related by pseudo-twofold symmetry. This property becomes particularly manifest in the $\{2, -1\}_t + \{1, -2\}_t$ Bragg rod (see Fig. 4 *B*), which has the observed shape corresponding to a cholesterol monolayer. A contribution to the x-ray structure factors of the two very similar yet symmetry-unrelated trilayers to the $\{2, -1\}_t + \{1, -2\}_t$ Bragg rod accounts for its observed shape but for minor modulations. The other reflections of the monohydrate phase, $\{2, 0\}_t + \{0, 2\}_t$ and $\{1, 2\}_t + \{2, 1\}_t$, superimpose on those of the rectangular phase.

A simple mechanism by which the monohydrate trilayer phase may develop from the rectangular bilayer phase is depicted and described in detail in Fig. 4 *D*. It essentially involves, first, a displacement along the direction of the diagonal $\pm(a + b)$ by half the axial repeat $\pm 0.5(a + b)$ of every second row of molecules of the rectangular bilayer phase or, alternatively, the molecules in every second row are to be rotated by 180° about their long axes. The second step is a minor shift of double rows along the direction $(-a + b)$. This transition, the barrier to which can be lowered by the presence of lattice defects, brings about a change in the layer structure that can be stabilized by the hydrogen bonds formed between the intercalated water molecules and the sterol OH groups.

CONCLUSIONS

The GIXD studies performed on ultrathin films of cholesterol, stigmasterol, and cholesterylacetate on water revealed crystallites with high lateral coherence in a motif that incorporates a 2-D rectangular unit cell of dimensions $\sim 10 \times 7.5$ Å^2. The cholesterol and the stigmasterol monolayers, each of trigonal symmetry and low crystallinity, transform, upon compression, into trilayers. Stigmasterol, upon monolayer collapse, forms a highly crystalline trilayer in an arrangement similar to the macroscopic crystals of stigmasterol-hemihydrate obtained from solution. The compressed cholesterol film, on the other hand, is composed of a highly crystalline bilayer in the 10×7.5 Å^2 lattice and a disordered cholesterol top layer. This film then transforms into a crystalline trilayer phase with the structural features of the 3-D monohydrate crystal and thus has a layer of ordered occluded water.

The crystallization process of cholesterol in the human body occurs in the presence of many other components such as bile salts in gallstones and various lipids in arteriosclerotic plaques. It has been proposed that cholesterol separates and nucleates out of supersaturated cholesterol solutions (Small and Shipley, 1974). The possibility that cholesterol assumes an unknown crystalline filamentous phase before evolving into plate-like monohydrate crystals has been raised in the study of model bile and human gall bladder bile from cholesterol stone patients (Konikoff et al., 1992). In accordance with these observations, GIXD studies of Langmuir films of some cholesterol-phospholipid mixtures (Lafont et al., 1998) have indicated that in cholesterol: DPPC mixtures with a ratio higher than 1:1, cholesterol separates out of the mixture and crystallizes in the form of the trigonal monolayer phase as described above, whereas at a ratio higher than 2:1, the cholesterol also crystallizes to form the rectangular bilayer phase, which has similar *d*-spacings as those of the filamentous cholesterol crystals

FIGURE 4 GIXD patterns of a cholesterol film on water in the compressed state ($A = 16$ Å^2), having undergone three expansion-compression cycles between $A = 16$ and 50 Å^2 within 1 h. (*A*) GIXD scans $I(q_{xy})$ measured 2 h after the 1-h preparation. The indices $\{h, k\}_m$, $\{h, k\}_b$, and $\{h, k\}_t$ specify the q_{hk} positions of the Bragg peaks corresponding to the trigonal monolayer (Fig. 1), the rectangular bilayer (Fig. 2), and the triclinic monohydrate trilayer, respectively. (*B*) The observed (×) and calculated (——) Bragg rod scans $I(q_z)$ of a trilayer phase of cholesterol monohydrate. (*C*) Cholesterol trilayer arrangement containing a water layer lies between the top and central layers. The H_2O and sterol OH groups are denoted by red circles. (*D*) Model of an intralayer cholesterol phase transition from the rectangular 10×7.6 Å^2 unit cell structure of the bilayer to the oblique 12.4×12.4 Å^2 unit cell structure of the trilayer, as viewed down their long molecular axes, that have similar tilt angles. Note the similarity in length of the diagonal $a \pm b$ in the rectangular phase (12.6 Å) and of the *a* and *b* axes in the monohydrate phase (12.4 Å). The two-layer structures are aligned so that the 2_1 *b* axis of the bilayer phase and the pseudo 2-fold axis along *a*-*b* of the monohydrate phase are parallel, denoted by symmetry direction. Thus, any transformation in one layer of the rectangular phase could, by symmetry, occur in an adjacent layer. For simplicity, the first step of the transition is presented as a plastic deformation of the layer involving a shift of successive molecular rows along the diagonal $-(a + b)$, by a distance $-n(a + b)/2$, for the *n*th row. This deformation is equivalent to shifting every second molecular row along the diagonal by $\pm(a + b)/2$, which corresponds to the length of an individual arrow. The sterol OH groups are colored red.

(vide supra). We therefore may speculate that the 2-D phases and phase transition pathways of cholesterol in ultrathin films as characterized here by GIXD may have bearing on cholesterol-rich structures and nucleation processes occurring at the onset of cholesterol crystallization in the human body.

We thank HASYLAB for synchrotron beamtime.

This work was supported by the Israel Science Foundation, the Kimmelmann Center, the DanSync program of the Danish Natural Science Research Council, and the European Community under TMR contract ERBFMGECT950059.

REFERENCES

Als-Nielsen, J., and K. Kjaer. 1989. X-ray reflectivity and diffraction studies of liquid surfaces and surfactant monolayers. *In* Phase Transitions in Soft Condensed Matter. T. Riste and D. Sherrington, editors. Plenum Press, New York. 113–138.

Bogren, H., and K. Larsson. 1963. An x-ray diffraction study of crystalline cholesterol in some pathological deposits in man. *Biochhim. Biophys. Acta.* 75:65–69.

Brown, D., and E. London. 1998. Structure and origin of ordered lipid domains in biological membranes. *J. Membr. Biol.* 164:103–114.

Craven, B. M. 1976. Cholesterol monohydrate. *Nature.* 260:727–729.

Craven, B. M. 1986. Cholesterol crystal structures: adducts and esters. *In* Handbook of Lipid Research, Vol. 4, The Physical Chemistry of Lipids. D. M. Small, editor. Plenum Press, New York. 149–182.

Guo, W., J. Morrisett, M. DeBakey, G. Lawrie, and J. Hamilton. 2000. Quantification in situ of crystalline cholesterol and calcium phosphate hydroxyapatite in human atherosclerotic plaques by solid-state magic angle spinning NMR. *Artheroscler. Thromb. Vasc. Biol.* 20:1630–1636.

Hsu, L. Y., and C. E. Nordman. 1983. Phase transition and crystal structure of the 37 form of cholesterol. *Science.* 220:604–606.

Jacquemain, D., S. G. Wolf, F. Leviller, M. Deutsch, K. Kjaer, J. Als-Nielsen, M. Lahav, and L. Leiserowitz. 1992. Two-dimensional crystallography of amphiphilic molecules at the air-water-interface. *Angew. Chem. Int. Ed. Engl.* 31:130–152.

Kaplun, A., Y. Talmon, F. M. Konikoff, M. Rubin, A. Eitan, M. Tadmor, and D. Lichtenberg. 1994. Direct visualization of lipid aggregates in native human bile by light-transmission and cryo-transmission electron-microscopy. *FEBS Lett.* 340:78–82.

Konikoff, F. M., D. S. Chung, J. M. Donovan, D. M. Small, and M. C. Carey. 1992. Filamentous, helical and tubular microstructures during cholesterol crystallization from bile: evidence that cholesterol does not nucleate classic monohydrate plates. *J. Clin. Invest.* 90:1155–1160.

Konikoff, F., D. Danino, D. Weihs, M. Rubin, and Y. Talmon. 2000. Microstructural evolution of lipid aggregates in nucleating model and human biles visualized by cryogenic transmission electron microscopy. *Hepatology.* 31:261–268.

Konikoff, F. M., H. Laufer, G. Messer, and T. Gilat. 1997. Monitoring cholesterol crystallization from lithogenic model bile by time-lapse density gradient ultracentrifugation. *J. Hepatol.* 26:703–710.

Lafont, S., H. Rapaport, G. J. Somjen, A. Renault, P. B. Howes, K. Kjaer, J. Als-Nielsen, L. Leiserowitz, and M. Lahav. 1998. Monitoring the nucleation of crystalline films of cholesterol on water and in the presence of phospholipid. *J. Phys. Chem.* 102:761–765.

Loomis, C. R., G. G. Shipley, and D. M. Small. 1979. The phase behavior of hydrated cholesterol. *J. Lipid Res.* 20:525.

Rapaport, H., I. Kuzmenko, M. Berfeld, R. Edgar, R. Popovits-Biro, I. Weissbuch, M. Lahav, and L. Leiserowitz. 2000. From nucleation to engineering of crystalline monolayer architectures at interfaces. *J. Phys. Chem. B.* 104:1399–1428.

Sheldrick, G. M. 1997. SHELX-97 Program for Crystal Structure Determination. University of Guttingen, Guttingen, Germany.

Shieh, H. S., L. G. Hoard, and C. E. Nordman. 1977. Crystal structure of anhydrous cholesterol. *Nature.* 267:287–289.

Shih, M. C., T. M. Bohanon, J. M. Mikrut, P. Zschack, and P. Dutta. 1992. X-ray-diffraction study of the superliquid region of the phase-diagram of a Langmuir monolayer. *Phys. Rev. A.* 45:5734–5737.

Simons, K., and E. Ikonen. 2000. Cell biology: how cells handle cholesterol. *Science.* 290:1721–1726.

Small, D. M. 1998. Progression and regression of arteriosclerotic lesions: insight from lipid physical biochemistry. *Arteriosclerosis.* 8:103–129.

Small, D. M., and G. G. Shipley. 1974. Physical chemistry basis of lipid deposition arteriosclerosis. *Science.* 185:222–229.

Somjen, G. J., G. Lipka, G. Schulthess, M. H. J. Koch, E. Wachtel, T. Gilat, and H. Houser. 1995. Behavior of cholesterol and spin-labeled cholestane in model bile systems studied by electron-spin-resonance and synchrotron x-ray. *Biophys. J.* 68:2342–2349.

Wang, D., and M. Carey. 1996. Characterization of crystallization pathways during cholesterol precipitation from human gallbladder biles: Identical pathways to corresponding model biles with three predominating sequences. *J. Lipid Res.* 37:2539–2549.